NANO LETTERS
Letter
Cite This: Nano Lett. XXXX, XXX, XXX−XXX
pubs.acs.org/NanoLett

Enzyme-Free Plasmonic Biosensor for Direct Detection of Neurotransmitter Dopamine from Whole Blood

Abraham Vázquez-Guardado,[†,∥] Swetha Barkam,[‡] Madison Peppler,[‡] Aritra Biswas,[†,∥] Wessley Dennis,[∥] Soumen Das,[‡] Sudipta Seal,[∥,‡,§,¶] and Debashis Chanda*[,†,∥,⊥]

[†]CREOL, College of Optics and Photonics, [‡]Advanced Materials Processing and Analysis Center, [§]College of Medicine, and [⊥]Department of Physics, University of Central Florida, Orlando, Florida 32816, United States

[∥]NanoScience Technology Center, University of Central Florida, Orlando, Florida 32826, United States

[¶]Materials Science and Engineering, University of Central Florida, Orlando, Florida 32816, USA

Supporting Information

ABSTRACT: Complex biological fluids without pretreatment, separation, or purification impose stringent limitations on the practical deployment of label-free plasmonic biosensors for advanced assays needed in point of care applications. In this work, we present an enzyme-free plasmonic neurotransmitter dopamine biosensor integrated with a microfluidic plasma separator. This integrated device allows the in-line separation of plasma directly from the bloodstream and channels it to the active detection area, where inorganic cerium oxide nanoparticles function as local selective dopamine binding sites through strong surface redox reaction. A thorough understanding and engineering of the nanoparticles is carried out to maximize its dopamine sensitivity and selectivity. We obtain detection of dopamine at 100 fM concentration in simulated body fluid and 1 nM directly from blood without any prior sample preparation. The detection selectivity is found to be at least five-times higher compared to the common interfering species. This demonstration shows the feasibility of the practical implementation of the proposed plasmonic system in detection of variety of biomarkers directly from the complex biological fluids.

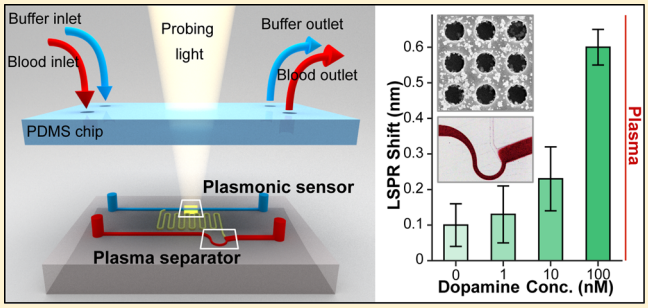

KEYWORDS: *Plasmonic biosensor, dopamine sensing, whole blood plasma separator, cerium oxide nanoparticles, integrated plasmonic−microfluidic chip, point of care applications*

Dopamine (DA) is an organic electrochemical neurotransmitter of paramount importance for the proper functioning of the neural system. Many neurological processes are associated with the active dopaminergic neurotransmission, for example, happiness, pleasure, cognition, and fine motor control. DA dysfunction, on the other hand, underlies the pathogenesis of several neurological disorders such as Parkinson's disease, Huntington's disease, depression, schizophrenia, or psychosis. In addition, it is also the biomarker for certain cancer strains such as pheochromocytoma,[1−3] neuroblastoma,[4] or paraganglioma.[5−8] For example, the plasma DA concentration in healthy adults ranges in the 0.1 nM,[9] and those with head and neck paragangliomas range up to 6 nM.[10] Therefore, detecting physiological and clinically relevant concentrations of DA with high sensitivity and selectivity is of great significance in basic pathophysiology research and drug development as well as in disease diagnosis and management.

Conventional analytical methods for DA detection are the enzyme-linked immunosorbent assay (ELISA) or the high-performance liquid chromatography (HPLC) as the analyte separation method coupled with fluorometry, coulometry, electrochemical, or mass spectroscopies as detection techniques.[11−15] Apart from the challenges associated with selectivity, sample consumption and analysis times, these methods require rigorous sample preparation to achieve the desired specificity and sensitivity (detection limit/time of 1 nM/100 min for ELISA and 4 pM/60 min for HPLC). In addition to the assay's high costs, these techniques require specialized laboratory equipment that prevents their translation to point of care applications where the access to high-end equipment is limited. With the aim to circumvent these aforementioned limitations, a wide range of alternative detection schemes have been previously reported, ranging from electrochemical to optical sensors. In the case of electrochemical detection, surface-modified microelectrodes are typically employed to enhance its detection capability;[16,17] for instance, electrodes are modified with active sensing materials such as metal or dielectric nanoparticles[18−20] or conductive polymers.[21,22] Electrochemical techniques have the

Received: October 22, 2018
Revised: November 21, 2018
Published: December 11, 2018

DOI: 10.1021/acs.nanolett.8b04253
Nano Lett. XXXX, XXX, XXX−XXX

advantages of low cost and rapid detection. However, there are limitations related to the intrinsic transduction mechanism, such as electro-polymerization leading to biofouling, rendering the device inactive. Another important concern is its reduced selectivity due to oxidizable DA metabolites and other compounds like ascorbic acid, which extensively interfere with the detection of DA as they have similar oxidizing potentials. Furthermore, the DA detection limits in buffer for most sensitive electrodes are around 1 to 0.1 nM[16,17] and 100 fM for field-effect-transistor design.[21] Optical DA sensors, on the other hand, are based on localized[23−26] or propagating[27−29] surface plasmon polariton (LSP and SPP, respectively), which are enzymatically functionalized to bind to DA. However, the main limitation in DA detection is its low mass (153.18 Da); hence, the lowest detection limits are still within 1 nM for most LSP and SPP and 200 fM for SPP with dedicated gold nanoparticle amplification mechanism.[30] Though previous publications demonstrate optical or electrochemical DA detection in buffer solutions[17−29] and off-line extracted serum/plasma,[16,19,31] the direct detection from biological body fluids, such as blood plasma, without sample preparation or purification, still remains challenging and unexplored.

In this work, we demonstrate an integrated enzyme-free DA biosensor composed of an active nanostructured plasmonic substrate (NPS) functionalized with oxygen-deficient cerium oxide nanoparticles (CNP) and a passive plasma separator microfluidic chip. The inorganic redox active CNP's surface acts as selective DA binding sites for the selective optical detection on the NPS.[32] Traditional affinity layers for DA detection, for example, those used in ELISA, employ antibodies or cellular membrane receptors. Such biological entities require specialized storage, handling, and preparation to maintain their affinity, sensitivity, and to avoid denaturation. In contrast, inorganic CNP do not suffer from these constraints, which enhance the robustness, shelf life, and reduce the assay cost considerably. When coupled to the microfluidic system, the proposed device extracts blood plasma directly from the inlet bloodstream without additional sample preparation or purification and allows optical readout on the CNP-coated NPS. In this initial demonstration, the detection limits of DA were measured 100 fM and 1 nM, in simulated body fluid and blood plasma, respectively. Furthermore, the sensor's response was compared with common interfering species, and it was found that DA's response exceeds at least by 5.3- and 20-times for ascorbic acid and epinephrine, respectively. No interference was observed for 3,4-dihydroxyphenylacetic acid (DOPAC).

The integrated device incorporates three essential elements: the sensitive NPS,[32,33] the selective CNP functionalizing the sensor's surface and the microfluidic plasma separator as shown in Figure 1a. The active NPS is formed by a gold hole-disk array coupled to an asymmetric photonic cavity fabricated using the nanoimprinting technique (see Supporting Information for more information), which proved to be robust and reliable in producing reproducible narrowband cavity-coupled plasmonic. This information is shown in Figure S1, where the statistical distribution of 930 spectral responses in 103 manually imprinted samples is summarized (mean plasmonic resonance at 823 nm with standard deviation of 16 nm). With the aid on an automated imprinting technique the sensor reproducibility could be dramatically improved. The NPS creates enhanced near-field via excitation of narrow line width

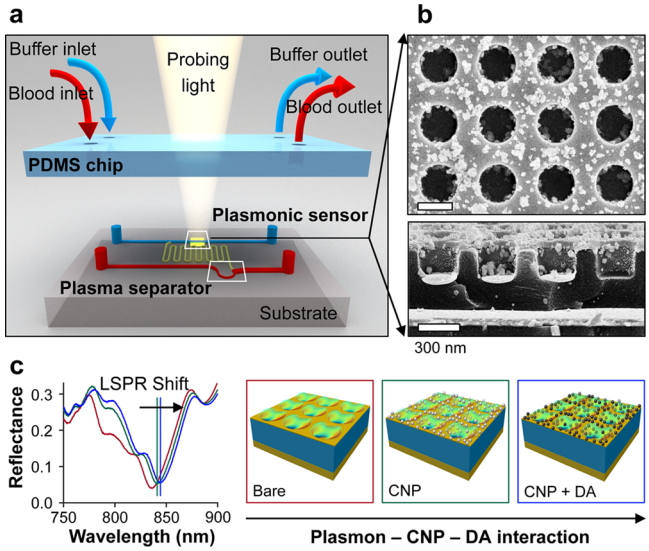

Figure 1. Integrated enzyme-free dopamine sensing. (a) Schematic representation of the integrated device composed of a plasmonic sensor coupled to a microfluidic chip containing the plasma separator module. (b) Top view and cross-section SEM of one CNP-functionalized plasmonic substrate. (c) Experimental spectra of one fabricated device (red), its spectral response after CNP coating (green), and after DA incubation at one representative concentration (blue). Right panels represent graphically these three phenomenological events.

hybrid cavity-coupled localized surface plasmonic resonance (LSPR), whose resonance location is determined by the hole/disk diameter and cavity thickness.[32−34] The LSPR is sensitive to minute perturbations in the optical density of the surrounding environment induced by subwavelength inorganic film accumulation or organic biomolecules, bulk refractive index, or isolated nanoparticles.[32,35] Any of these possible interaction scenarios induce an accumulation of polarization charges on the substrate producing the LSPR to redshift nonselectively.

The surface selectivity is introduced by binding the complementary analyte surfactant to the active plasmonic surface such as an antibody against the target antigen for selective binding. In this study, the NPS's surface is modified with CNP, which have strong affinity toward electroactive compounds such as DA.[36,37] Figure 1b shows a scanning electron microscope image of a representative CNP coated plasmonic surface. Upon mutual redox activity, DA binds on the CNP's surface inducing a change in the CNP effective refractive index.[36,38] This effect is manifested in the LSPR response, which experiences a resonance shift proportional to the overall surface coverage. This mechanism is observed in Figure 1c containing the reflectance spectra measured experimentally at three stages of the characterization process: bare plasmonic substrate, after CNP coating, and after CNP +DA coating (see Supporting Information for more details). The overall sensor response is determined by the LSPR shift from CNP to the DA binding state; see Figure 1c.

The passive microfluidic plasma separator chip exploits a series of cascaded hydrodynamic and biophysical effects. In the first effect, the Zweifach-Fung bifurcation law, a microfluidic channel that bifurcates into two outlets with asymmetric flow rate ratio, at least 2.5:1, imposes a selective drag force on red and white blood cells (BCs) toward the path with higher

DOI: 10.1021/acs.nanolett.8b04253
Nano Lett. XXXX, XXX, XXX−XXX

pressure.[39,40] As a result, the channel with large flow resistance carries the BCs-free plasma, while the one with low flow resistance carries the residual media containing the large density of BCs toward the waste reservoir outlet. Such a separation method is further amplified by the fact that BCs migrate toward the center of the flow channel, or blood vessel in biological systems, with cross-sections less than 300 μm leaving a BCs-free layer on the walls. Also known as the Fahraeus effect, its influence on BCs migration to the center increases as the channel contracts, a self-regulated effect exploited by the vascular system. Finally, inertial focusing permits BCs migration to the center due to the balance between lift and drag forces produced in channel bends.[41−43] Along with the Fahraeus effect the inertial focusing obtained by the contracting bent further enhances the plasma separation at the bifurcation (see Figure S4). The device channels the separated plasma toward the active plasmonic biosensing area as observed in Figure 1a where the spectroscopic optical interrogation takes place. The synergetic interaction among these elements enables efficient extraction of plasma from the complex biological fluids such as blood.

At the nano scale (3−5 nm diameter), CNP support the coexistence of Ce^{3+} and Ce^{4+} oxidation states on its surface forming oxygen vacancies in the crystal lattice.[36,44−46] These oxygen vacancies act like catalytic hotspots that induce unique redox reactions with electroactive compounds such as serotonin, epinephrine, DA, and norepinephrine.[36] Previous studies showed that due to the redox reaction CNP interaction with DA form charge complexes, thereby oxidizing dopamine.[36] This results in dopaquinone−CNP hybrid complexes with an intermediate semiquinone state observed as a red shift in the characteristic UV−visible spectra. The ratio Ce^{3+}/Ce^{4+} on the surface (CeSR) of CNP is the metrics for CNP redox activity, which regulates its enhanced catalytic property and controls the extent of reaction with different electrochemical compounds, that is, DA. To understand the CeSR effect toward DA interaction, two relatively different CNP compositions were prepared that exhibit different surface chemistry: CNP1 with CeSR > 1 and CNP2 with CeSR < 1 (see Supporting Information for more details). These two particles were carefully formulated to have similar spherical shape and size with diameter of 3−5 nm that differ only in their surface chemistry, see Figure S2a. The X-ray photoelectron spectroscopy (XPS) characterization shows that CNP1 has a CeSR of 2.57 and CNP2 has that of 0.68 as seen Figure S2b. The DA−CNP interaction is studied using in situ UV−visible spectro-electrochemistry analysis on both of these CeSR compositions (see Supporting Information for more details). This study helps to gauge the change in surface chemistry of CNP in the presence of dopamine by oxidizing the solution using an external potential applied to the CNP−DA solution.

Dopamine has two distinct absorption peaks corresponding to two oxidation states. In pristine unoxidized DA, an absorption peak at 281 nm dominates the UV−visible spectrum. An increasing external potential (0−0.8 V) oxidizes DA and a second absorption peak starts appearing at 390 nm, while the peak at 281 nm diminishes simultaneously, as observed in Figure 2a. Moreover, CNP1 (CeSR > 1; more Ce^{4+} on the surface) solution has a Ce^{4+} extinction peak at 290 nm. Upon oxidation, its Ce^{4+} surface concentration further increases indicated by the increase in the peak height of the 290 nm extinction peak in Figure 2c. On the other hand,

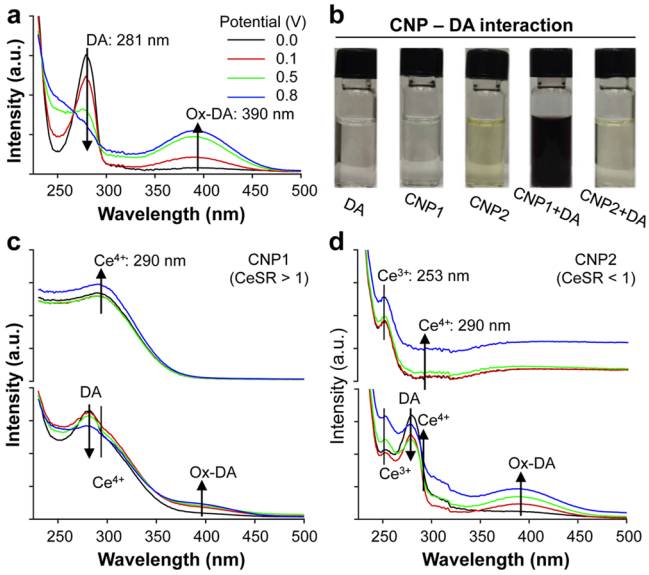

Figure 2. CNP−dopamine interaction analysis in situ. (a) Dopamine UV−visible spectro-electrochemical analysis as a function of external potential: 0, 0.1 0.5, and 0.8 V. (b) Optical images of dopamine and its interaction with CNP1 (CeSR > 1) and CNP2 (CeSR < 1). UV−visible spectro-electrochemical analysis of pristine (top) and mixed with dopamine (bottom) for (c) CNP1 and (d) CNP2 as a function of oxidizing potential: 0, 0.1, 0.5, and 0.8 V.

CNP2 (CeSR < 1; more Ce^{3+} on the surface) solution has a distinctive Ce^{3+} peak at 253 nm with negligible Ce^{4+} extinction peak. Upon oxidation, the increase in Ce^{4+} concentration is manifested as a baseline upshift resulting in the formation of Ce^{4+} as observed in Figure 2d. Now, when CNP1 interacts with DA, the free unoxidized state population decreases (drop of extinction peak at 281 nm), whereas the absorption intensity of Ce^{4+} peak remains unchanged as observed in Figure 2c. It is important to notice that the absence of free oxidized DA, whose extinction peak does not strongly show at 390 nm, suggests its absorption onto the CNP surface, which indicates a strong interaction between CNP1 and DA. However, when CNP2 interacts with DA, the spectra indicate a superposition of oxidized CNP2 (observed by the increase in the Ce^{4+} at 290 nm) and DA (population inversion as in Figure 2a) individually. Such a behavior indicates hardly any interaction upon increasing the oxidation potential as shown in Figure 2d. In other words, the oxidation behavior of CNP2 and dopamine are mutually independent of each other.

In addition, the DA−CNP complex formation was visually observed. Initially both CNP formulations and DA appear clear. Once mixed, there is an immediate change in color for CNP1+DA (dark brownish see Figure 2b) compared to hardly any change observed in CNP2+DA as shown in Figure 2b. This suggests the rapid formation of charge transfer complex, in the form of nanoparticle coating, with a decrease of free unoxidized DA. As previously suggested, the oxidation of dopamine by CNP leads to formation of reactive dopaquinone intermediates, which bind to the surface of CNP. This distinctly suggests that the oxidation followed by the binding on surface of CNP leads to a decline of free DA concentration, thereby indicating the preference of DA oxidation for CNP with CeSR > 1.[36] The CNP (from here on refereeing to CNP1) affinity toward DA is exploited as an enzyme-free DA inorganic ligand in this on-chip biosensing demonstration.

DOI: 10.1021/acs.nanolett.8b04253
Nano Lett. XXXX, XXX, XXX−XXX

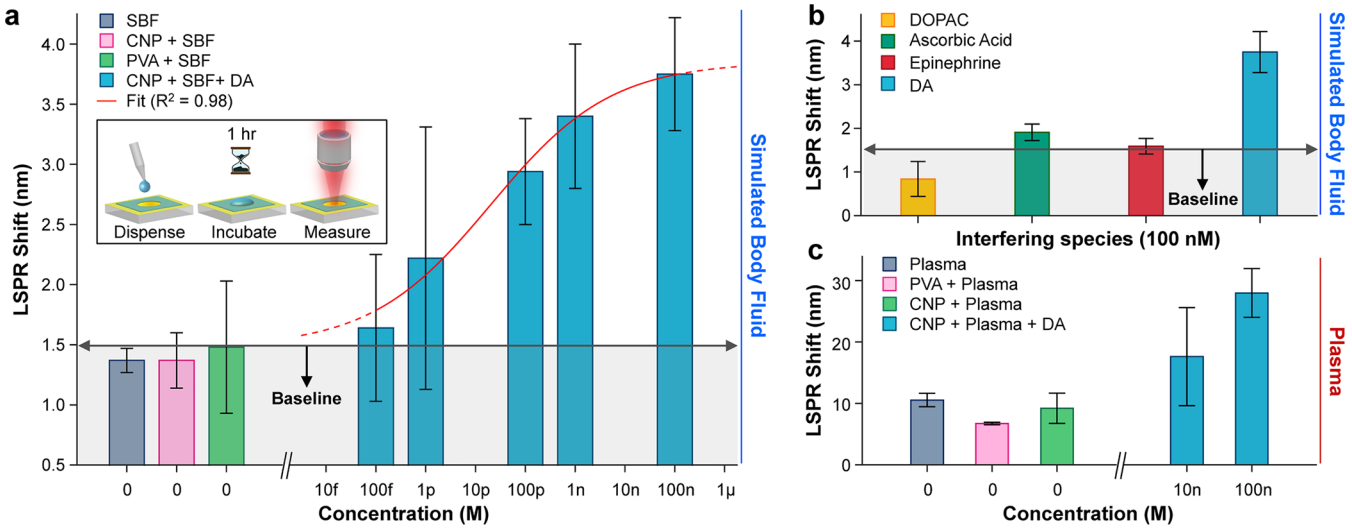

Figure 3. Characterization in aqueous solution. (a) Dopamine sensing characterization in SBF from 100 fM to 100 nM. Control experiments represent the sensors response in the absence of CNP coating and buffer effect. Inset represents the characterization flowchart. The shaded area represents the baseline of the sensor. (b) Interfering species response test: DOPAC, ascorbic acid, epinephrine, and dopamine at 100 nM in SBF. (c) Dopamine sensing feasibility test in spiked sheep plasma. Control experiments represent the sensors response in the absence of CNP coating and buffer (plasma) effect. Error bars represent the standard deviation from the mean (n = 9).

The first characterization is to validate the DA detection capability on this CNP-functionalized NPS. NPS were coated with poly(vinyl alcohol) (PVA) stabilized CNP. To improve uniformity and area coverage, denser CNP layer was used, which in turn improved the sensor reproducibility and sensitivity. The optimization was done using different PVA:CNP solution ratio and spin coating cycles producing different surface coverage as observed in Figure S3a, followed by 100 nM DA incubation (see Supporting Information for more details). It was observed that the denser the surface coverage due to additional coating cycles, the larger the spectral shift; however, considerable CNP agglomeration accompanied this process as well. Such an effect hinders the sensitivity of the device due to the decline in oxidizability efficiency produced by the lower surface area of agglomerated CNP, which is observed in the sensor's response plotted in Figure S3b. Considering this trade-off, eight coating cycles were found to be optimum.

Upon surface functionalization optimization, the sensor's response was characterized. DA at various concentrations was incubated in simulated body fluid (SBF), a buffer whose ion concentration is close to that of human blood plasma, as well as different control samples and plotted in Figure 3a (see Supporting Information for more details). DA in SBF with concentration between 100 fM and 100 nM produced a plasmonic shift according to its concentration and follows a standard sigmoid response fitted curve (R^2 = 0.98) in Figure 3a. The estimated limit of detection is 45 fM determined when the standard sigmoid curve falls to 10% of its maximum (EC10), which is an order of magnitude smaller than that of previous SP-based DA sensing using plasmonic nanoparticles as signal amplification.[30] In addition, three control measurements were carried out: SBF incubation on an uncoated sensor, CNP coated sensor, and just PVA coated sensor. All these responses produced a residual response introduced by the combination of the sensor substrates and its functionalizing constituents in the absence of DA, which fall below the detection limit. Such a residual response of $\Delta\lambda \approx 1.48$ nm observed in the shaded area in Figure 3a is the baseline of the device, which works as the reference to account positive response from the sensor. Then the sensor's response was tested against common DA interfering species, such as DOPAC, ascorbic acid, and epinephrine. It is clear that CNP's response to DOPAC is negligible as observed in Figure 3b, while it is at least 5.3- and 20-times larger than ascorbic acid and epinephrine, respectively, which indicates its selectivity toward DA.

Next, DA detection feasibility in a more complex matrix, such as blood plasma, was tested. Two concentrations of DA, 10 and 100 nM, were spiked in purchased sheep plasma and then incubated on the sensors (see Supporting Information for more details). In this particular situation, plasma, which is composed of a wide range of proteins, undergoes electrostatic surface binding on the sensor's surface. This undesirable effect introduces a larger background as observed in the plasmonic shift in Figure 3c in presence and absence of DA, compared to those in Figure 3a and b. Nevertheless, the sensor produced two distinguishable signals in response to the DA. These characterizations demonstrate the enzyme-free detection of DA in buffers, such as SBF, as well as in complex biological fluids such as blood plasma.

The final demonstration corresponds to the direct detection of DA in plasma obtained from whole blood. The integrated device incorporates a microfluidic module that performs in-line blood plasma separation as shown in Figure 1a. The microfluidic channel footprint, adapted from previous reports,[39,47] is shown in Figure S4. This module extracts a portion of the blood plasma and directs it toward the active CNP coated NPS. The microfluidic chip is laminated on a previously fabricated and CNP functionalized plasmonic substrate and held together with the help of an acrylic clamp as observed in Figure S5. Two inlets provide access of phosphate-buffered saline (PBS) buffer and whole blood into the chip. The external fluid distribution configuration is drawn in Figure S6. In first instance, the PBS solution is flown into the channel at ~0.02 mL/min to stabilize the sensor, producing a baseline ($\Delta\lambda_0$) response. Next, the blood flow is introduced at ~0.1 mL/min to produce plasma separation, as

DOI: 10.1021/acs.nanolett.8b04253
Nano Lett. XXXX, XXX, XXX−XXX

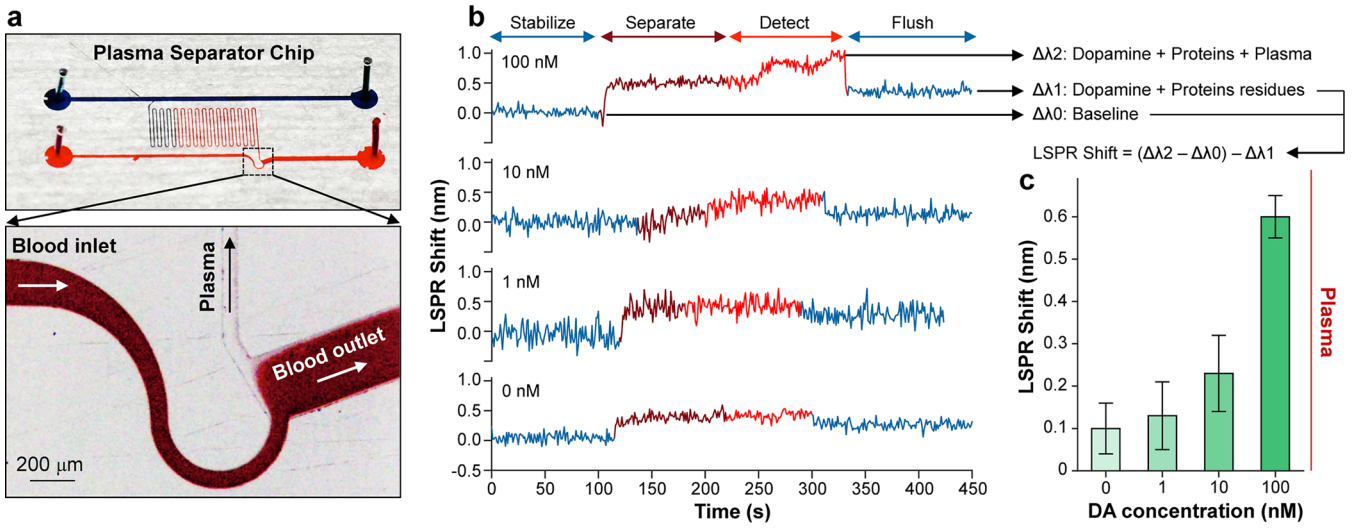

Figure 4. Dopamine detection from whole blood. (a) Microfluidic chip containing the in-line plasma separation. Colored channels are represented with colored solutions for illustration purposes. Bottom panel shows plasma separation demonstration on one device tested with *HCT 22.3%* flowing at ~0.1 mL/min. (b) DA detection directly from in-line separated plasma for four samples, 100 nM, 10 nM, 1 nM, and control (without DA), in whole blood with *HCT 22.3%*. Four events are observed: stabilization in buffer, plasma separation, plasma incubation, and flush. (c) Sensor's response for DA detection in whole blood through the integrated plasma separator chip for three samples at 100 nM, 10 nM, and 1 nM and a control. Error bars indicate the sensorgrams standard deviation from the mean.

seen in Figure 4a, bottom panel. This high-speed plasma solution is flown for approximately one to 2 min until full plasma separation occurs. Then the flow is stopped to allow further interaction between the freestanding DA in the separated plasma solution and the CNP attached to the sensor's surface. During the plasma separation and incubation steps, proteins bind to the surface as observed in Figure 3c and Figure 4b resulting in the inherent sensor baseline response after the flushing step. At the same time, DA is captured on the CNP surface proportional to the total free DA in the solution producing a total sensor response of $\Delta\lambda_2$. The total sensor response at this state will correspond to $\Delta\lambda_2-\Delta\lambda_0$. Finally, the plasma is flushed with PBS cleaning the proteins from the sensor surface. However, residual protein electrostatically attached to the surface produces background spectral shift ($\Delta\lambda_1$). The sensor response toward DA is then estimated as the total response minus the final background: $(\Delta\lambda_2-\lambda_0)-\Delta\lambda_1$. Figure 4b shows the LSPR time evolution during the assay in the integrated device for three DA concentrations, 100 nM, 10 nM, and 1 nM, along with one control sample without DA. The combined sensor response for these four samples is plotted in Figure 4c, which indicates detection of DA in the range of 1 nM. This initial detection range typically benefit in the detection of DA in dopamine-secretting paragangliomas tumors whose typical levels are from 1 to 363 nM concentrations.[8] Standard analytical methods for DA detection, see Table S1, reach low detection limits or selectivity at the trade-off between long assay times and laborious sample preparations protocols. In contrast to other detection techniques like ELISA or HPLC where extensive sample preparation is required, the proposed method preforms detection directly from whole blood. The preliminary 1 nM detection limit and 5 min detection time from whole blood are comparable and well within the standard norms. These systematic measurements show that with additional design optimization the detection limit can be further reduced. Moreover, this principle can be straightforwardly extrapolated for the direct detection of various biomarkers directly from blood even in the presence of various interfering species.

In this work, we present for the first time the demonstration of DA detection from a complex biological fluid using an enzyme-free DA plasmonic biosensor integrated with a dynamic blood plasma separator chip. The relevance of this work not only relies on the enzyme-free selective detection of DA in the plasmonic sensor, but also the successful detection from a complex matrix such as whole blood without sample preparation in an integrated microfluidic device. This concept opens up the opportunity for more complex label-free assays to be developed to target potential antigen and biomarkers in raw biological fluids using sensitive plasmonic substrates. However, performing the detection of DA, as well as other antigen or biomarkers, in plasma without preparation or purification is susceptible to inherent protein fouling from the high protein content in biological fluids, and hence, further work is still needed to establish a generalized detection protocol. Overall, the proposed label-free plasmonic biosensors have proven their potential in low-concentration detection of biomarkers based on a low cost integrated platform for future point of care applications.

■ ASSOCIATED CONTENT

Supporting Information

The Supporting Information is available free of charge on the ACS Publications website at DOI: 10.1021/acs.nanolett.8b04253.

Cerium oxide nanoparticles synthesis and characterization, device fabrication, optical characterization, microfluidic chip fabrication and specifications, fluid sample preparations, supporting figures and tables (PDF)

■ AUTHOR INFORMATION

Corresponding Author

*E-mail: debashis.chanda@ucf.edu. Phone: +1 407 823 4575.

DOI: 10.1021/acs.nanolett.8b04253
Nano Lett. XXXX, XXX, XXX−XXX

ORCID

Abraham Vázquez-Guardado: 0000-0002-0648-5921
Sudipta Seal: 0000-0002-0963-3344

Author Contributions

A.V.-G. and D.C. conceived the idea. A.V.-G., S.D., and S.B. designed the experiments. A.V.-G., S.B., M.P., and A.B. performed the experiments. A.V.-G. and W.D. developed the Labview interface. A.V.-G. analyzed the data. A.V.-G. and D.C. cowrote the manuscript. S.B. and S.S. edited the manuscript. S.S. and D.C. contributed with materials/analysis tools.

Notes

The authors declare no competing financial interest.

■ ACKNOWLEDGMENTS

This work was supported by the National Science Foundation under Grant No. ECCS/EPMD-1808045 and Northrop Grumman University Research Program. A.V.-G. acknowledges support from the Consejo Nacional de Ciencia y Tecnologia (CONACyT).

■ REFERENCES

(1) Dubois, L. A.; Gray, D. K. *World J. Surg.* **2005**, *29* (7), 909−913.
(2) Tippett, P. A.; McEwan, A. J.; Ackery, D. M. *Clin. Endocrinol.* **1986**, *25* (4), 401−410.
(3) Januszewicz, W.; Wocial, B.; Januszewicz, A.; Gryglas, P.; Prejbisz, A. *Blood Pressure* **2001**, *10* (4), 212−216.
(4) Anagnoste, B.; Freedman, L. S.; Goldstein, M.; Broome, J.; Fuxe, K. *Proc. Natl. Acad. Sci. U. S. A.* **1972**, *69* (7), 1883−1886.
(5) Van Der Horst-Schrivers, A. N. A.; Osinga, T. E.; Kema, I. P.; Van Der Laan, B. F. A. M.; Dullaart, R. P. F. *Anticancer Res.* **2010**, *30* (12), 5153−5158.
(6) Soh, A. W. E.; Kek, P. C. *Intern. Med.* **2012**, *51* (6), 613−618.
(7) Yi, J. W.; Oh, E. M.; Lee, K. E.; Choi, J. Y.; Koo, D. H.; Kim, K. J.; Jung, K.-C.; Kim, S.-Y.; Youn, Y.-K. *J. Korean Surg. Soc.* **2012**, *82* (6), 389−393.
(8) Eisenhofer, G.; Goldstein, D. S.; Sullivan, P.; Csako, G.; Brouwers, F. M.; Lai, E. W.; Adams, K. T.; Pacak, K. *J. Clin. Endocrinol. Metab.* **2005**, *90* (4), 2068−2075.
(9) Goldstein, D. S.; Eisenhofer, G.; Kopin, I. J. *J. Pharmacol. Exp. Ther.* **2003**, *305* (3), 800−811.
(10) Van Der Horst-Schrivers, A. N. A.; Osinga, T. E.; Kema, I. P.; Van Der Laan, B. F. A. M.; Dullaart, R. P. F. *Anticancer Res.* **2010**, *30* (12), 5153−5158.
(11) Hubbard, K. E.; Wells, A.; Owens, T. S.; Tagen, M.; Fraga, C. H.; Stewart, C. F. *Biomed. Chromatogr.* **2010**, *24* (6), 626−631.
(12) Raggi, M. A.; Sabbioni, C.; Nicoletta, G.; Mandrioli, R.; Gerra, G. *J. Sep. Sci.* **2003**, *26* (12−13), 1141−1146.
(13) Kim, J.; Jeon, M.; Paeng, K.-J.; Paeng, I. R. *Anal. Chim. Acta* **2008**, *619* (1), 87−93.
(14) Yoshitake, T.; Yoshitake, S.; Fujino, K.; Nohta, H.; Yamaguchi, M.; Kehr, J. *J. Neurosci. Methods* **2004**, *140* (1−2), 163−168.
(15) Hows, M. E. P.; Lacroix, L.; Heidbreder, C.; Organ, A. J.; Shah, A. J. *J. Neurosci. Methods* **2004**, *138* (1−2), 123−132.
(16) Wang, Y.; Zhang, Y.; Hou, C.; Liu, M. *RSC Adv.* **2015**, *5*, 98260−98268.
(17) Feng, X.; Zhang, Y.; Zhou, J.; Li, Y.; Chen, S.; Zhang, L.; Ma, Y.; Wang, L.; Yan, X. *Nanoscale* **2015**, *7* (6), 2427−2432.
(18) Baron, R.; Zayats, M.; Willner, I. *Anal. Chem.* **2005**, *77* (6), 1566−1571.
(19) Liu, K.; Pang, H.; Zhang, J.; Huang, H.; Liu, Q.; Chu, Y. *RSC Adv.* **2014**, *4* (17), 8415−8420.
(20) Lin, Y.; Chen, C.; Wang, C.; Pu, F.; Ren, J.; Qu, X. *Chem. Commun. (Cambridge, U. K.)* **2011**, *47* (4), 1181−1183.
(21) Lee, J. S.; Oh, J.; Kim, S. G.; Jang, J. *Small* **2015**, *11* (20), 2399−2406.
(22) Zhong, M.; Teng, Y.; Pang, S.; Yan, L.; Kan, X. *Biosens. Bioelectron.* **2015**, *64* (c), 212−218.
(23) Rithesh Raj, D.; Prasanth, S.; Vineeshkumar, T. V.; Sudarsanakumar, C. *Sens. Actuators, B* **2016**, *224*, 600−606.
(24) Choi, J.-H.; Lee, J.-H.; Oh, B.-K.; Choi, J.-W. *J. Nanosci. Nanotechnol.* **2014**, *14* (8), 5658−5661.
(25) Choi, Y.; Choi, J.-H.; Liu, L.; Oh, B.-K.; Park, S. *Chem. Mater.* **2013**, *25* (6), 919−926.
(26) Biswal, J.; Misra, N.; Borde, L. C.; Sabharwal, S. *Radiat. Phys. Chem.* **2013**, *83*, 67−73.
(27) Sebők, D.; Csapó, E.; Preočanin, T.; Bohus, G.; Kallay, N.; Dékány, I. *Croat. Chem. Acta* **2013**, *86* (3), 287−295.
(28) Kumbhat, S.; Shankaran, D. R.; Kim, S. J.; Gobi, K. V.; Joshi, V.; Miura, N. *Chem. Lett.* **2006**, *35* (6), 678−679.
(29) Matsui, J.; Akamatsu, K.; Hara, N.; Miyoshi, D.; Nawafune, H.; Tamaki, K.; Sugimoto, N. *Anal. Chem.* **2005**, *77* (13), 4282−4285.
(30) Cao, Y.; McDermott, M. T. *bioRxiv* **2018**, 1−24.
(31) Yadav, S. K.; Rosy; Oyama, M.; Goyal, R. N. *J. Electrochem. Soc.* **2014**, *161* (1), H41−H46.
(32) Vázquez-Guardado, A.; Smith, A.; Wilson, W.; Ortega, J.; Perez, J. M.; Chanda, D. *Opt. Express* **2016**, *24* (22), 25785−12.
(33) Chanda, D.; Shigeta, K.; Truong, T.; Lui, E.; Mihi, A.; Schulmerich, M.; Braun, P. V.; Bhargava, R.; Rogers, J. A. *Nat. Commun.* **2011**, *2*, 479−7.
(34) Vázquez-Guardado, A.; Safaei, A.; Modak, S.; Franklin, D.; Chanda, D. *Phys. Rev. Lett.* **2014**, *113* (26), 263902.
(35) Li, J.; Ye, J.; Chen, C.; Li, Y.; Verellen, N.; Moshchalkov, V. V.; Lagae, L.; Van Dorpe, P. *ACS Photonics* **2015**, *2* (3), 425−431.
(36) Hayat, A.; Andreescu, D.; Bulbul, G.; Andreescu, S. *J. Colloid Interface Sci.* **2014**, *418* (C), 240−245.
(37) Bulbul, G.; Hayat, A.; Liu, X.; Andreescu, S. *RSC Adv.* **2016**, *6*, 60007−60014.
(38) Ghosh Chaudhuri, R.; Paria, S. *Chem. Rev.* **2012**, *112* (4), 2373−2433.
(39) Tripathi, S.; Kumar, Y. V. B.; Agrawal, A.; Prabhakar, A.; Joshi, S. S. *Sci. Rep.* **2016**, *6*, 26749.
(40) Yang, S.; Ündar, A.; Zahn, J. D. *Lab Chip* **2006**, *6* (7), 871−880.
(41) Martel, J. M.; Toner, M. *Sci. Rep.* **2013**, *3* (1), 209−8.
(42) Di Carlo, D.; Edd, J. F.; Irimia, D.; Tompkins, R. G.; Toner, M. *Anal. Chem.* **2008**, *80* (6), 2204−2211.
(43) Seo, J.; Lean, M. H.; Kole, A. *Appl. Phys. Lett.* **2007**, *91* (3), 033901−033904.
(44) Reed, K.; Cormack, A.; Kulkarni, A.; Mayton, M.; Sayle, D.; Klaessig, F.; Stadler, B. *Environ. Sci.: Nano* **2014**, *1*, 390−405.
(45) Karakoti, A. S.; Monteiro-Riviere, N. A.; Aggarwal, R.; Davis, J. P.; Narayan, R. J.; Self, W. T.; McGinnis, J.; Seal, S. *JOM* **2008**, *60* (3), 33−37.
(46) Das, S.; Dowding, J. M.; Klump, K. E.; McGinnis, J. F.; Self, W.; Seal, S. *Nanomedicine* **2013**, *8* (9), 1483−1508.
(47) Prabhakar, A.; Kumar, Y. V. B. V.; Tripathi, S.; Agrawal, A. *Microfluid. Nanofluid.* **2015**, *18*, 995−1006.

DOI: 10.1021/acs.nanolett.8b04253
Nano Lett. XXXX, XXX, XXX−XXX